Journal of Power Sources 201 (2012) 159–163

Contents lists available at SciVerse ScienceDirect

Journal of Power Sources

journal homepage: www.elsevier.com/locate/jpowsour

Short communication

Performance and analysis of a novel polymer electrolyte membrane fuel cell using a solution based redox mediator

R. Singh[a], A.A. Shah[a,*], A. Potter[b], B. Clarkson[b], A. Creeth[b], C. Downs[b], F.C. Walsh[a]

[a] Energy Technology Research Group, School of Engineering Sciences, University of Southampton, Highfields, Southampton SO17 1BJ, United Kingdom
[b] ACAL Energy Ltd., The Heath Business and Technical Park, Runcorn, Cheshire WA7 4QX, United Kingdom

ARTICLE INFO

Article history:
Received 15 June 2011
Received in revised form 3 October 2011
Accepted 21 October 2011
Available online 28 October 2011

Keywords:
Polymer electrolyte membrane fuel cell
Polyoxometalate
Liquid redox cathode
Platinum-free
Mathematical model

ABSTRACT

The cost and availability of platinum, together with degradation phenomena that are directly or indirectly caused by the use of a precious-metal catalyst, are major obstacles to the commercialization of incumbent polymer electrolyte membrane fuel cell (PEMFC) technologies. The Flowcath® fuel cell technology is a highly promising alternative to the conventional PEMFC that avoids many of these issues. While the anode resembles that of a conventional cell, the novel cathode employs a liquid-based polyoxometalate redox mediator and is entirely free of any precious metals. A transition-metal based redox centre within the polyoxometalate undergoes reversible reduction in the cathode and is regenerated externally using air. In this paper, the performance of the cell for different catholyte flow rates and polyoxometalate concentrations is described and a first model is developed and validated. The voltage losses are quantified and compared to the values for a conventional cell employing a standard membrane electrode assembly.

1. Introduction

There are several impediments to realising the commercial benefits of proton exchange membrane (PEM) fuel cells, notably cost and longevity. The use of platinum in conventional PEM fuel cells, particularly in the performance-limiting cathode, not only raises the cost of the cells but leads directly to degradation phenomena such as dissolution and sintering of the catalyst particles. A PEM fuel cell that replaces the conventional cathode with a flow-through platinum-free carbon electrode was developed by ACAL Energy Ltd. (Fuel Cells, Patent: WO/2007/110663). This novel structure utilises a polyoxometalate (POM) containing a transition metal ion redox centre, such as V^{IV}/V^{V}, in place of hexavalent tungsten or molybdenum. The basic structure of the POM anions used in the Flowcath® system is of type $[XM_{12-m}V_mO_{40}]^{n-}$, where X is commonly P, Si or B, M is typically molybdenum or tungsten, and n is the charge of the anion. The fundamental reaction in the cathode is:

$$(XM_{12-m}V^{V}_{m}O_{40})^{n-} + xe^{-} + xH^{+} \longrightarrow (H_xXM_{12-m}V^{V}_{m-x}V^{IV}_{x}O_{40})^{n-} \quad (1)$$

where V^{IV} and V^{V} are the reduced and oxidised (vanadium) species, respectively, and x is between 1 and m depending on the extent of the reaction. In a separate regenerator, the POM is oxidised in the solution phase before it is recycled to the electrode: $(H_xXM_{12-m}V^{IV}_{m}O_{40})^{n-} + (x/4)O_2 \rightarrow (XM_{12-m}V^{V}_{m}O_{40})^{n-} + (x/2)H_2O$.

In this paper, the performance of the system is presented for the first time. To aid understanding of the performance, a first model of the cell (focused on the cathode processes) is developed and the cell voltage losses for different flow rates and POM concentrations are studied.

2. Experimental and modelling details

2.1. Experimental

A single 25 cm^2 cell was tested with the standard ACAL catholyte (POM and de-ionised water) at varying flow rates and catholyte concentrations. The cell build incorporated a porous carbon cathode (RVC supplied by ERG) material for the reduction of the catholyte, a commercially available 50 μm Nafion based membrane (supplied by Ion Power) and a gas diffusion layer (GDL) with a flow field and microporous layer at the anode. These were encapsulated by two carbon blocks (Le Carbone) and current collectors (gold coated copper plates), and held together with two steel blocks bolted to a set torque. The catholyte solution was heated to 80 °C and pumped through the cell (KNF diaphragm pump) where the temperature was maintained with a heater rod. H_2 (99.999% purity,

* Corresponding author. Present address: School of Engineering, University of Warwick, Coventry CV4 7AL, United Kingdom. Tel.: +44 (0)24 761 51676; fax: +44 (0)24 76 418922.
E-mail address: Akeel.Shah@warwick.ac.uk (A.A. Shah).

0378-7753/$ – see front matter © 2011 Elsevier B.V. All rights reserved.
doi:10.1016/j.jpowsour.2011.10.078

BOC) was supplied to the anode and a back pressure of 1.6 bar maintained throughout. Electrochemical measurements were taken by connecting the cell to a potentiostat (Biologic) and carrying out polarisation experiments at 500 mA s^{-1} to evaluate the cell voltage. The polarisation curves were taken (with the catholyte in the same oxidation state) at 50, 100 and 150 ml min^{-1} for POM concentrations of 0.45, 0.3 and 0.2 M. The catholyte concentration was reduced by the addition of water. Excess water was removed by evaporation in order to maintain a constant concentration during testing.

2.2. Mathematical model

Since the conventional anode is well-characterised, attention is focused on the complex cathode processes. The anode is treated implicitly through boundary conditions and, along with contact resistances, as an additional resistance R_a that gives rise to a cell voltage loss IR_a, where I is the applied cell current (load). This is a reasonable first approximation since the activation and mass transport losses in a conventional anode are small and often assumed to be zero. The domain to be modelled is enclosed in the dotted rectangle in Fig. 1. Based on the POM used in the experiments, reaction (1) is represented in the following manner:

$$V^{V} + e^{-} \longrightarrow V^{IV} \tag{2}$$

where V^{IV} and V^{V} refer to the redox centres of the POM. The species considered are dissolved H_2O, H^+, V^{IV}, V^{V} and a counterion. Certain simplifying, (but reasonable) first-approximations are adopted: (i) two-dimensional through-plane flow (see Fig. 1); (ii) a dilute-solution approximation [1]; (iii) laminar, incompressible flow; (iv) cathodic and anodic charge transfer coefficients of 0.5; (v) the POM solution is returned to the electrode from the regenerator at a constant POM concentration; (vi) reduction of vanadium species within the POM molecule is a one electron process (for a similar system Odyakov et al. [4] demonstrated that this assumption is valid).

Using the Nernst–Planck equation [1], the mass balances for H_2O, V^{V}, V^{IV} and H^+ in the porous carbon cathode take the form:

$$\nabla\cdot\left(-\epsilon^{3/2}D_i\nabla c_i - \frac{z_i c_i \epsilon^{3/2} D_i}{RT}F\nabla\phi_e - c_i\frac{d_p^2\epsilon^3}{K\mu(1-\epsilon)^2}\nabla p\right) = -\frac{\nu_i j_c}{F} \tag{3}$$

where ϵ is the porosity; ϕ_e is the ionic potential; R, T and F are the molar gas constant, temperature and Faraday's constant, respectively; c_i, D_i, z_i and ν_i are the concentration, diffusion coefficient (subject to a Bruggeman correction), charge and stoichiometric coefficient (in reaction (2)) of species i; and j_c is the cathode transfer current density. The counterion concentration is given by the electroneutrality condition: $\sum_i z_i c_i = 0$. The electrolyte velocity $\vec{v}$ (in the last term on the left-hand side) is given by Darcy's law in combination with the Kozeny–Carman law for the electrode permeability [2], where μ is the dynamic viscosity of the liquid, d_p is the mean pore diameter and K is the Kozeny–Carman constant. Ionic charge conservation in the cathode electrolyte can be expressed as follows [3]:

$$j_c = -\nabla\cdot\left(\frac{F^2}{RT}\nabla\phi_e\sum_i z_i^2 D_i\epsilon^{3/2}c_i + F\sum_i z_i D_i^{eff}\nabla c_i\right) \tag{4}$$

and the electronic potential ϕ_s in the porous electrode and the current collector is given by Ohm's law:

$$-\sigma_s^{\text{eff}}\nabla^2\phi_s = -j_c, \quad -\sigma_c\nabla^2\phi_s = 0 \tag{5}$$

where σ_s^{eff} (σ_c) is the effective conductivity of the cathode (collector).

The driving forces for the movement of dissolved protonated water in the membrane are concentration, potential and pressure gradients. The concentration c_{H_2O} satisfies the mass balance[5]:

$$-\nabla\cdot(D_w^{eff}\nabla c_{H_2O}) + \nabla\cdot(\vec{v}c_{H_2O}) = 0, \quad \vec{v} = -\frac{k_\phi}{\mu}Fc_{H^+}\nabla\phi_e - \frac{k_p}{\mu}\nabla p \tag{6}$$

in which D_w^{eff} is the effective water diffusion coefficient, $\vec{v}$ is the liquid velocity (given by Schloegl's equation), k_ϕ is the electrokinetic permeability and k_p is the hydraulic permeability. Incompressibility, i.e., $\nabla\cdot\vec{v} = 0$, is assumed. Charge conservation is again given by Ohm's law in the form [5]: $-\sigma_m\nabla^2\phi_e = 0$, where $\sigma_m = F^2D_{H^+}^m c_{H^+}/(RT)$ is the membrane conductivity.

The rate of reaction (2) is assumed to follow the Butler–Volmer law (with equal transfer coefficients):

$$j_c = \epsilon Fk(c_{V^{IV}}^s)^{1/2}(c_{V^{V}}^s)^{1/2}\left\{\exp\left(\frac{F\eta}{2RT}\right) - \exp\left(-\frac{F\eta}{2RT}\right)\right\} \tag{7}$$

where k is the reaction rate constant and $\eta = \phi_s - \phi_e - E^0$ is the overpotential in the cathode. The reversible open circuit electrode potential is estimated using the Nernst equation: $E^0 = E^{0\prime} + (RT/F)\ln(c_{V^V}^s/c_{V^{IV}}^s)$, in which the effect of pH variations is neglected. The quantities c_i^s are the concentrations of the vanadium species at the liquid-solid interfaces in the porous cathode. They can be related to the bulk values, c_i, by approximately balancing the rate of reaction with the rate of diffusion of reactant to the electrode surface at steady state [3]:

$$c_i^s = \frac{c_i + \epsilon k e^{-F(\phi_s-\phi_e-E^0)/(2RT)}(c_{V^{IV}}/\gamma_{V^V} + c_{V^V}/\gamma_{V^{IV}})}{1 + \epsilon k\left(e^{-F(\phi_s-\phi_e-E^0)/(2RT)}/\gamma_{V^V} + e^{F(\phi_s-\phi_e-E^0)/(2RT)}/\gamma_{V^{IV}}\right)} \tag{8}$$

where i is V^{V} or V^{IV}. At the reaction surface, a stagnant boundary layer is incorporated. Following [6], the thickness of the boundary layer, δ, is inversely proportional to the square root of the local electrolyte speed, $|\vec{v}|$, i.e., $\delta = k_\delta/\sqrt{|\vec{v}|}$, which gives $\gamma_i = D_i/(k_\delta/\sqrt{|\vec{v}|})$, where k_δ is a constant of proportionality.

Fig. 1 shows the boundary conditions. At the cathode inlet, the liquid electrolyte enters with a prescribed bulk velocity. At the outlet, a fully-developed flow condition is used. The current, I enters uniformly through current collectors on the cathode side. The complementary boundary condition at $x = x_0$ is derived from a one-dimensional charge balance across the anode catalyst layer. Conservation of charge demands that $\sigma_e\,\partial_x\phi_e + \sigma_s\,\partial_x\phi_s = I/a$, where σ_s and σ_e are the electronic and ionic conductivities in the anode catalyst layer, respectively. Applying this equation to the membrane/catalyst layer interface (zero electron flux) gives the condition at $\partial\Omega_1$ in Fig. 1. The ionic conductivity σ_e is approximated as $\sigma_e = \epsilon_e^{3/2}F^2D_{H^+}c_{H^+}$ where ϵ_e is the volume fraction of ionomer in the anode.

3. Results and discussion

The system of equations and boundary conditions was solved using COMSOL Multiphysics. Due to the lack of available data for this new system, it was necessary to estimate certain parameters in the model: the reaction constant, k, the proportionality constant for the diffusion boundary layer thickness, k_δ, and the resistance R_a. The parameter estimation (implemented in Matlab) was performed rigorously through a nonlinear least-squares fit of six simulated polarisation curves for different POM concentrations and flow rates to experimental data obtained under the same conditions. Six data points from each of the six curves were used to form the least-squares sum. The resulting values are given in Table 1, along with the other parameter values. The inlet concentrations of V^{IV}, V^{V}

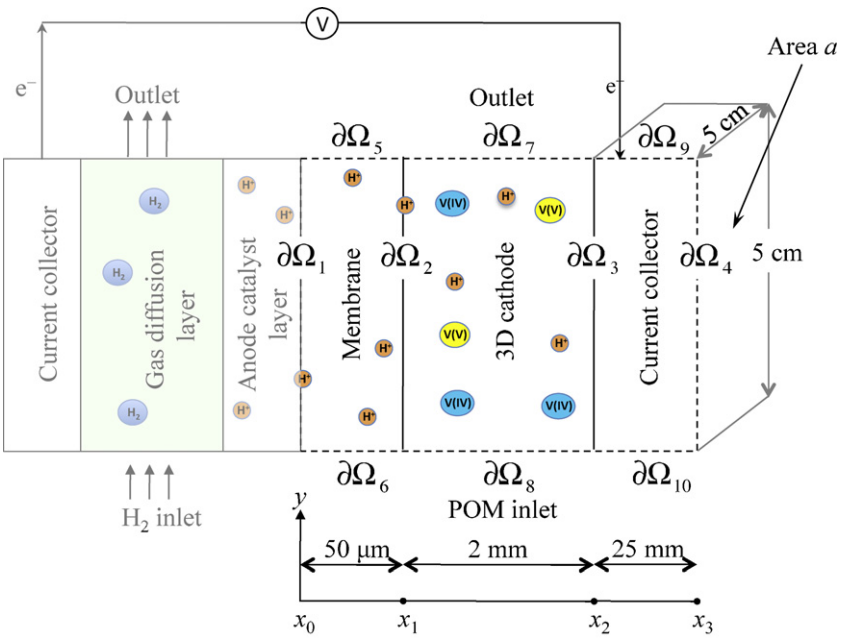

Boundary conditions

$\partial\Omega_1$: $\sigma_e \nabla\phi_e \cdot \vec{n} = I/a$; $\nabla p \cdot \vec{n} = 0$

$\partial\Omega_2$: Reactant/electron insulation

$\partial\Omega_3$: Reactant/proton insulation

$$\nabla p \cdot \vec{n} = 0$$

$\partial\Omega_4$: $-\sigma_c \nabla\phi_s \cdot \vec{n} = I/a$

$\partial\Omega_5$ and $\partial\Omega_6$: Reactant insulation

$$\sigma_e \nabla\phi_e \cdot \vec{n} = 0$$

$\partial\Omega_7$:

$$\nabla c_i \cdot \vec{n} = 0; \quad p = p_{out}$$

$\partial\Omega_8$:

$$c_i = c_i^0; \quad \vec{v} = (0, v_{in})$$

$\partial\Omega_9$ and $\partial\Omega_{10}$:

$$-\sigma_c \nabla\phi_s \cdot \vec{n} = I/a$$

Fig. 1. A schematic of the Flowcath® cell and of the components modelled in this report (enclosed in the dotted line).

(strictly speaking of the redox centres), H^+ and H_2O were calculated based on the POM concentration, the pH of the solution, and the degree of reduction (DOR), defined as $c_{V^{IV}}/(c_{V^{IV}} + c_{V^V})$. For example, for a β M POM concentration and a DOR of d, the V^{IV} concentration is βdm M, where m is the number of V redox centres. For reasons of proprietary, the actual V^{IV} and V^V concentrations are not shown.

Fig. 2 compares the experimental and simulated polarisation curves at different electrolyte inlet flow rates with a fixed POM concentration and at different POM concentrations with a fixed inlet flow rate. The model captures the variations in the cell voltage with changes in the POM concentration and flow rate well, both qualitatively and quantitatively. The simulated polarisation curves in Fig. 2(b) overpredict the cell voltage at low current densities, particularly as the POM concentration is increased. This is likely to be due to the assumption that the reaction rate and Nernst potential are independent of the pH (the precise stoichiometry of the cathode reaction is still under study). Analysis of a similar POM system [4] has shown that the pH of the POM solution decreases with an increase in the POM concentration for a fixed DOR. In other words, the stoichiometry of the cathode reaction with respect to protons depends in a complex manner on both the POM concentration and the DOR; the present model does not incorporate this dependence.

The open circuit voltage for the cell (Fig. 2) is approximately 0.83 V, which is around 0.1 V lower than that of a PEM fuel using a standard membrane electrode assembly (MEA). The theoretical open-circuit potential for a conventional cell, around 1.23 V at 298 K, is not attained due to a mixed potential at the cathode and, to a lesser extent, H_2 crossover [12]. For a 0.45 M POM solution and an inlet flow rate of 150 ml min^{-1}, the total voltage losses at 0.7 and 1 A cm^{-2} are 0.279 V and 0.359 V, respectively. The equivalent numbers for a standard cell (also with a 50 μm PFSA membrane and a 25 cm^2 active area) can be considerably higher, particularly at moderate to high current densities. For example, a cell operating at 70 °C on fully humidified air (stoichiometric coefficient of 5) and H_2 at 0% RH (as in the present system) with a platinum loading of 0.57 mg cm^{-2} [7] exhibited voltage losses of 0.400 V and 0.583 V at 0.7 and 1 A cm^{-2}, respectively. The best performance was attained by humidifying both channels at 80% RH, leading to voltage losses of 0.321 V at 0.7 A cm^{-2} and 0.457 V at 1 A cm^{-2} – still significantly higher. On the other hand, a state-of-the-art cell employed by Gasteiger et al. [13] with a 25 μm PFSA membrane and a 50 cm^2 active area (platinum loading of 0.4 mg cm^{-2}) exhibited voltage drops of 0.24 V and 0.3 V at the same current densities. The power densities at 0.7, 1 and 1.2 A cm^{-2} for the conventional cell in [7] were 0.445, 0.488 and 0.171 W cm^{-2}, respectively. In the present

Table 1
Default parameter values for the simulations (inlet concentrations are based on a 0.3 M POM solution).

Symbol	Quantity	Size
ϵ_e	Ionomer volume fraction in anode	0.35
ϵ	Porosity of the cathode	0.85
$D_{V^{IV}}$	V^{IV} diffusion coefficient in electrolyte	5.65×10^{-10} m^2 s^{-1} [8]
$D_{V^{V}}$	V^{V} diffusion coefficient in electrolyte	5.65×10^{-10} m^2 s^{-1}[8]
D_{H_2O}	Water diffusion coefficient in electrolyte	2.3×10^{-9} m^2 s^{-1} [9]
D_w	Water diffusion coefficient in the membrane	5.75×10^{-10} m^2 s^{-1} [10]
$D^m_{H^+}$	Proton diffusion coefficient in the membrane	1.4×10^{-9} m^2 s^{-1} [5]
D_{H^+}	Proton diffusion coefficient in the electrolyte	9.7×10^{-9} m^2 s^{-1} [11]
σ_c	Current collector conductivity	8.33×10^4 S m^{-1}
σ_s^{eff}	Porous cathode conductivity	600 S m^{-1}
K	Kozeny–Carman constant: porous electrode	5.55
κ_ϕ	Electrokinetic permeability: membrane	1.13×10^{-19} m^2 [5]
κ_p	Hydraulic permeability: membrane	1.58×10^{-18} m^2 [5]
k	Rate constant for reaction (2)[a]	4.7×10^{-3} s^{-1}
k_δ	Diffusion boundary layer thickness constant[a]	3.67×10^{-7} m$^{3/2}$ s^{-1}
R_a	Anode and contact resistance[a]	0.0069 Ω
$E_0{}'$	Formal potential: V^{IV}/V^V	1.004 V *vs.* NHE
c_f	Fixed charge site (sulfonate) concentration	1800 mol m^{-3}
$c^0_{H_2O}$	Water concentration at cathode inlet	4.2×10^3 mol m^{-3}
$c^0_{H^+}$	Initial H^+ concentration	500 mol m^{-3}
T	Cell temperature	80 °C
p_{out}	Cathode outlet pressure	100 kPa

[a] Estimate based on a nonlinear least-squares analysis.

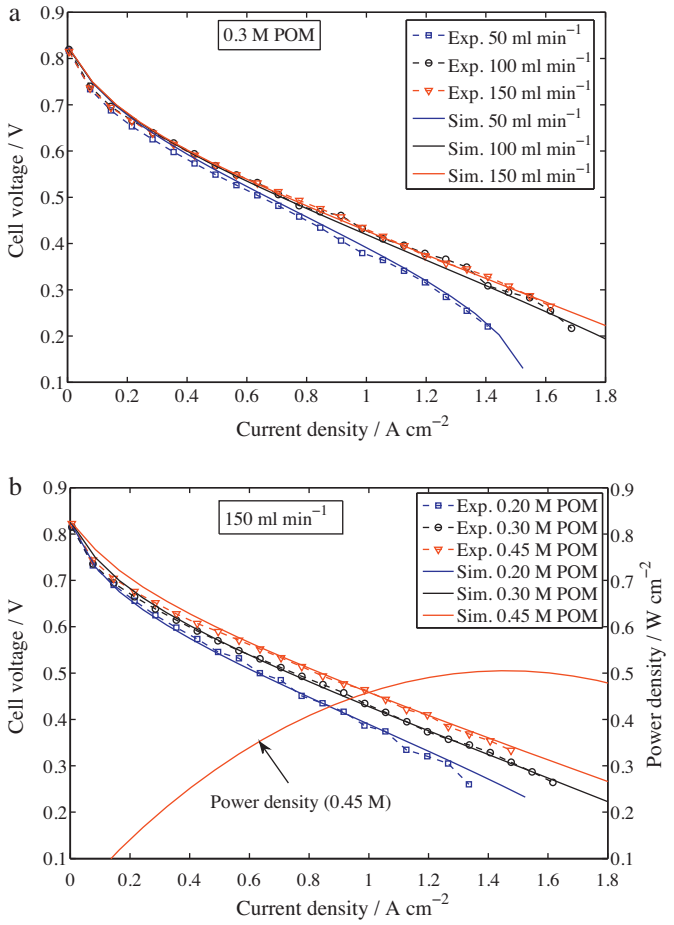

Fig. 2. Comparisons of the experimental and simulated polarisation curves at different electrolyte inlet velocities and different POM concentrations.

system, the equivalent values for a 0.45 M POM concentration and 150 ml min^{-1} flow rate were 0.378, 0.461 and 0.493 W cm^{-2}, demonstrating superior performance at high current densities (typical of automobile applications) and comparable performance at moderate current densities. The state-of-the-art system in [13] achieved power density values of 0.50, 0.66 and 0.76 W cm^{-2} and did not suffer severe mass-transport losses up to 1.2 A cm^{-2} (see below). Improvements are clearly required in order to match this level of performance. It is important to bear in mind, however, that the performance of the test cell used in this work is far from optimal and that significant improvements are achievable, particularly with respect to the ohmic losses incurred in the membrane, electrodes and current collectors, the flow distribution through the electrodes, contact resistances and the POM solution composition.

Fig. 2(a) shows that the performance improves dramatically with an increase in the flow rate from 50 to 100 ml min^{-1} but only mildly with an increase from 100 to 150 ml min^{-1}. The flow rate influences both the characteristic residence time for reaction, $\tau_R = h/v_y$ (where h is the electrode height and v_y is the y component of the velocity) and the characteristic diffusion time through the boundary layer, $\tau_D = \delta^2/nD_i = k_\delta^2/nv_yD_i$, where n is a constant that depends on the pore geometry. The timescale τ_R increases rapidly as the flow rate is reduced, which leads to greater depletion of the V^V reactant at a fixed current density and, therefore, higher average cathode overpotentials. This effect is compounded by the simultaneous increase in τ_D, which leads to a greater deviation of the surface concentration from the bulk value. The derivatives of both time scales with respect to v_y are proportional to $1/v_y^2$, suggesting that improvements in performance decay quadratically (or at least diminish) as the flow rate is increased.

In order to measure the ohmic losses across the cathode and membrane, simulations were performed for a series of flow rates between 50 and 1000 ml min^{-1} with a POM concentration of 0.45 M. The ohmic losses were defined as $IR_{ohm}/A = \overline{E}^0 - |\overline{\eta}| - V_{cell}$, where bars denote spatial averages of the quantities in the cathode and A is the active surface area. For a sufficiently high flow rate, mass transport losses are essentially eliminated and R_{ohm} gives a measure of the overall ohmic resistance; mass transport and activation losses in the conventional anode are small and the ohmic losses are incorporated in R_a. The change in R_{ohm} decreased rapidly as the flow rate increased from 50 and 250 ml min^{-1}, beyond which only small changes were observed. A flow rate of 1000 ml min^{-1} yielded a qualitative prediction of $R_{ohm} = 0.173\ \Omega\ cm^2$. The ohmic losses in a conventional cell are highly dependent on the membrane conductivity and dimensions, the operating temperature and relative humidity [7], the volume fraction of ionomer in the catalyst layers [14], and the conductive properties and dimensions of the electrodes and plates. Reported values for the ohmic resistance in state-of-the-art conventional cells generally fall in the range 50–100 mΩ cm^2 [13,14]. These measurements, taken from current-interrupt or impedance spectroscopy experiments, cannot be compared directly to the R_{ohm} value given above, which is a highly qualitative approximation. Gasteiger et al. [13] reported a cell ohmic resistance of 45–55 mΩ cm^2 (using current-interrupt) for a PEFC employing a 25 μm Nafion membrane and operating at 80 °C with fully humidified hydrogen and air inlet streams. In their cell, which used a microporous layer in the cathode, mass transport limitations were not dominant even at the upper limit of 1.2 A cm^{-2}. Makharia et al. [14] estimated the ohmic resistance of a PEFC employing a 50 μm thick Nafion membrane and

operating at 80 °C and 100% relative humidity to be approximately 60 mΩ cm^2 (from an impedance spectroscopy analysis); however, this resistance did not include a separately calculated catalyst-layer electrolyte resistance to proton transport, which was estimated to be around 100 mΩ cm^2. The total 'ohmic' resistance of around 160 mΩ cm^2 is very close to the value of R_{ohm} given above.

The condition of a liquid-saturated membrane (at the cathode) in the present system appears to maintain a high membrane conductivity, with the effect of Schroeder's paradox likely to be a contributing factor. Although the ohmic losses are considerably reduced in a conventional cell by full humidification of both channels, severe mass-transport losses caused by liquid–water flooding can limit the maximum (limiting) current density [7]. To ameliorate this problem, micro-porous layers and optimised operating/flow conditions are used [13,15]. Such losses are eliminated altogether in the present cell without the need for contact-angle control using hydrophobic agents and/or additional components such as an MPL (which can degrade [16]) and/or water management strategies, as well as higher flow rates/pressures in the channels. As is seen from the simulated curve in Fig. 2(b), moderately high power densities up to and beyond 1.8 A cm^{-2} are readily achievable in the present unoptimised cell.

4. Conclusions

Experimental and modelling results for a novel PEM fuel cell employing a solution based cathode have demonstrated that the cathode overpotentials under typical operating conditions can be lower than those in a cell employing a standard MEA. Improvements are clearly required, nevertheless, to match the performance of state-of-the-art cells. It is important to reiterate, however, that the test cell studied used in this work has not been optimised in terms of the individual components, anode humidification, contact resistances, POM solution composition and the flow distribution in the cathode, amongst other considerations. In this sense, the results are highly promising. One of the advantages of using a flow-through electrode is the ability to exert control over the reactant distributions by careful design of the flow. In conventional cells, mass transport is limited by the diffusion of O_2 to the reaction sites through the gas diffusion and catalyst layers, which is more difficult to control and can be hindered by the slow gas–solid reaction and liquid–water flooding at high current densities and/or high relative humidities.

The model results in this paper shows that the losses incurred at the anode and through contact resistances (approximated by IR_a) are non-negligible and that the effects of pH changes on the reaction kinetics, Nernst potential and DOR are potentially significant. Work is ongoing to explicitly incorporate both the anode and the influence of pH and to investigate the stoichiometry of the cathode reaction in detail. Future studies based on a full-cell model will examine voltage losses in greater detail under different operating conditions and design parameters.

Acknowledgement

The authors would like to acknowledge funding for the present work from the Technology Strategy Board, UK (TSB Grant TP/BH039G 100773).

References

[1] J. Newman, Electrochemical Systems, Prentice Hall, Engelwood Cliffs, NJ, 1991.
[2] R.A. Freeze, J.A. Cherry, Groundwater, Prentice-Hall, NJ, 1979.
[3] A.A. Shah, M.J. Watt-Smith, F.C. Walsh, Electrochim. Acta 53 (2008) 8087–8100.
[4] V.F. Odyakov, E.G. Zhizhina, K.I. Matveev, J. Mol. Catal. A 158 (2000) 453–456.
[5] D.M. Bernadi, M.W. Verbrugge, AIChE J. 37 (1991) 1151–1163.
[6] C.V. Chrysikopoulos, P.Y. Hsuan, M.M. Fyrillas, K.Y. Lee, J. Hazard. Mater. 97 (2003) 245–255.
[7] Y.H. Park, Investigation of the performance and water transport of a polymer electrolyte membrane (PEM) fuel cell, PhD Thesis, Texas A & M University, 2007, pp. 87–90 (Chapter 5).
[8] C.X. Li, Y. Zhang, K.P. O'Halloran, J.W. Zhang, H.Y. Ma, J. Appl. Electrochem. 39 (2009) 421–427.
[9] R. Mills, J. Phys. Chem. 77 (1973) 685–688.
[10] T.E. Springer, T.A. Zawodinski, S. Gottesfeld, J. Electrochem. Soc. 138 (1991) A2334–A2341.
[11] J. Choi, N. Hirota, M. Terazima, J. Phys. Chem. A 105 (2001) 12–18.
[12] J. Zhang, Y. Tang, C. Song, J. Zhang, H. Wang, J. Power Sources 163 (2006) 532–537.
[13] H.A. Gasteiger, S.S. Kocha, B. Sompalli, F.T. Wagner, Appl. Catal. B: Environ. 56 (2005) 9–35.
[14] R. Makharia, M.F. Mathias, D.R. Baker, J. Electrochem. Soc. 152 (2005) A970–A977.
[15] R.P. Ramasamy, E.C. Kumbur, M.M. Mench, W. Liu, D. Moore, M. Murthy, Int. J. Hydrogen Energy 33 (2008) 3351–3367.
[16] S. Zhang, X. Yuan, H. Wang, W. Merida, H. Zhu, J. Shen, S. Wu, J. Zhang, Int. J. Hydrogen Energy 34 (2009) 388–404.